Materials Science & Engineering A 730 (2018) 66–72

Contents lists available at ScienceDirect

Materials Science & Engineering A

journal homepage: www.elsevier.com/locate/msea

Effect of Ta and Nb additions in arc-melted Co-Ni-based superalloys: Microstructural and mechanical properties

A.M.S. Costa[a,*], J.P. Oliveira[b,f], M.V. Salgado[c], C.A. Nunes[c], E.S.N. Lopes[d], N.V.V. Mogili[a], A.J. Ramirez[b], A.P. Tschiptschin[e]

[a] Brazilian Nanotechnology National Laboratory (CNPEM), Rua Giuseppe Máximo Scolfaro, 10.000 Polo II de Alta Tecnologia de Campinas, CEP 13083-970 Campinas, SP, Brazil
[b] Department of Materials Science and Engineering, The Ohio State University, 1248 Arthur E. Adams Drive, Columbus, OH 43221, USA
[c] Escola de Engenharia de Lorena (EEL), Universidade de São Paulo (USP), Polo Urbo-Industrial Gleba AI-6, Caixa Postal 116, CEP 12602-810 Lorena, São Paulo, Brazil
[d] Department of Materials Engineering, Faculty of Mechanical Engineering, State University of Campinas, CEP 13083-860 Campinas, São Paulo, Brazil
[e] Department of Metallurgical and Materials Engineering, University of São Paulo (USP), CEP 05508-900 São Paulo, SP, Brazil
[f] UNIDEMI, Departamento de Engenharia Mecânica e Industrial, Faculdade de Ciências e Tecnologia, Universidade Nova de Lisboa, Caparica, Portugal

ARTICLE INFO

Keywords:
Co-Ni-based superalloys
Ta and Nb additions
γ/γ′ structure
Microstructural characterization
Hot compression tests, yield stress

ABSTRACT

The current work characterizes the microstructure and mechanical properties of two arc melted Co-Ni-based superalloys containing in atomic percent: 1) Co-40Ni-10Al-7.5W-10Cr-3Ta-0.06B-0.6 C and 2) Co-40Ni-10Al-7.5W-10Cr-3Nb-0.06B-0.6 C. These two materials named 3Ta and 3Nb, respectively, were characterized by X-Ray diffraction analysis, differential scanning calorimetry, scanning electron microscopy, energy dispersive spectroscopy, electron backscatter diffraction and transmission electron microscopy. Furthermore, compression tests were performed from room temperature up to 1000 °C. The 3Ta and 3Nb alloys showed different as-cast microstructures that were confirmed by microstructural characterization and Scheil simulations. The phase transformation temperatures of minor phases were measured and calculated using a thermodynamic approach and some discrepancies observed on the calculated γ′-*solvus* temperatures reflect that the thermodynamic description of γ′ phase does not take into account the strong partition effect of Ta, Nb and Ti into γ′. As shown by DSC results, the γ′ phase was stable for both alloys up to 1000 °C, being the main reason for the 3Ta and 3Nb alloys to keep the yield stress above 500 MPa.

1. Introduction

The demand for high temperature materials that can replace conventional Ni-based superalloys has led to the development of new materials, which possess similar or improved mechanical properties at high temperatures. For Ni-based superalloys, the existence of a coherent fine cuboidal $L1_2$-ordered γ′ intermetallic phase, precipitated in a solid solution γ matrix, and the low energy γ/γ′ interface are considered two of the key factors that contribute to the high-temperature strength and thermal stability of these alloys [1].

Co-based superalloys are potential substitutes for Ni-based superalloys, due to their higher melting point. Usually, in polycrystalline Co-based superalloys, the controlled addition of carbon allows for the formation of carbides. Under appropriate heat treatment conditions, these carbides can be finely dispersed in the alloy matrix to hinder dislocation motion and grain boundary sliding. Cr, W, Mo, Nb and Ta can provide solid solution strengthening, and these are also known to be carbide forming elements. Typical carbide compounds are M_6C, $M_{23}C_6$, M_7C_3, M_3C_2 and MC where M can be one of the aforementioned alloying elements [2,3]. In binary systems such as Co-Ti and Co-Ta [4,5] and ternaries ones such as Co-Ti-V and Co-W-Ge [6,7] it was reported the formation of the γ/γ′ structure, similar to what was observed in Ni-based superalloys. However, the phase stability of the γ′ phase was low in these systems resulting in inferior high temperature mechanical properties.

In 2006, Sato et al. [8] identified a ternary γ′-Co_3(Al,W) phase, with a $L1_2$ structure in Co-Al-W alloys. Similar finding were presented before by Lee [9] who studied the effects of different contents of refractory elements such as Ta, Nb, Mo and W in Co-4Al-X (in wt% and X being one of the refractory elements) on the phase stability of the system. One of the main concerns about the Co-Al-W based superalloys is related to a very narrow γ + γ′ phase field [8] and the γ′ phase was considered as metastable [10]. To overcome this drawback, Ni additions have been used to widen the γ + γ′ field and increase the γ′-*solvus* as well. As

* Corresponding author.
E-mail address: alex.costa@lnnano.cnpem.br (A.M.S. Costa).

https://doi.org/10.1016/j.msea.2018.05.078
Received 14 December 2017; Received in revised form 16 April 2018; Accepted 21 May 2018
Available online 22 May 2018
0921-5093/

shown by Ruan et. al [11], Co-Ti-V base superalloys alloyed with Ni presented the γ′-*solvus* temperature 82 °C higher than the base material and improved the yield strength when compared to the traditional Co-base superalloy (named Mar-M302) between 700 and 1000 °C. This way, Co-Ni-Al-W-based superalloys have been studied and some works pay attention to phase stability issues and found that controlled additions of Ta, Nb, Ti, and V are effective to increase the phase stability of the γ-γ′ microstructure, the γ′-volume fraction and the γ′-*solvus* temperature [12–16].

Due to the addition of several alloying elements, computational thermodynamic calculations can help to understand their effects on phase formation, composition and stability, which are crucial to accelerate the introduction of these materials into specific applications and reduce the necessary time to design new alloys. Looking into Co-Al-W and Co/Ni-Al-W-X (X = Ta, Nb, Cr, Mo, Ti, B, C) based superalloys for multicomponent materials a significant effort has been made to predict how the phase stability is affected by thermal exposure, solidification path, microsegregation behavior, alloying elements on the γ-γ′ structure and transformation temperatures [10,17–22].

The present article characterizes the microstructure and mechanical properties of two multi-components arc melted Co-Ni-based superalloys: i) Co-40Ni-10Al-7.5W-10Cr-3Ta-0.06B-0.6 C (at%) and ii) Co-40Ni-10Al-7.5W-10Cr-3Nb-0.06B-0.6 C (at%). Moreover, this characterization work is supported by thermodynamic calculations.

2. Experimental procedures

Two Co-Ni-based superalloys, named as 3Ta and 3Nb alloys, were produced by arc melting. Pure elements were used to melt ingots of 20 g under argon atmosphere. In order to ensure a good chemical homogeneity of the alloys, each ingot was remelted five times. The composition, in at%, of each alloy is depicted in Table 1.

Differential scanning calorimetry (DSC) was performed in the as-cast alloys to determine their transformation temperatures. Samples of 100 mg were heated at a rate of 10 °C/min from room temperature to 1500 °C. The solidification path including the phase transformation and phase composition of both materials was predicted by Scheil calculations using *Thermo-Calc*® and the TCNI8 database was selected to perform the simulations [23]. The calculated and experimental γ′-*solvus* temperatures were compared.

Hardness tests were performed on as-cast 3Ta and 3Nb alloys. The conditions were a load of 500 gf and 30 s of dwell time. 20 indentations were performed and the average was determined.

Isothermal compression tests to determine the 0.2% yield stress of 3Ta and 3Nb alloys were performed. The results obtained for the 3Ta and 3Nb were compared with two Ni-based superalloys (Mar-M247 and B1914), which were mechanically tested in the same experimental conditions using a thermo-mechanical simulator Gleeble 3800. The diameter and length of the samples are 4 mm and 6 mm, respectively. The hot compression tests were performed at a strain rate of 4.5×10^{-4} s^{-1} from room temperature to 1000 °C. The sample was heated at a rate of 15 °C/s up to the deformation temperature followed by 60 s of soaking time to ensure isothermal homogeneity of sample. Thermal conditions during the tests were recorded by a type K thermocouple welded into the central part of cylindrical samples. All samples were deformed up to 10% (0.1 true strain) and to reduce the friction during hot deformation, a Ta foil with the thickness of 0.1 mm and a Ni-based lubricant were placed between the sample and anvils.

Table 1
Chemical composition of the produced Co-Ni-based superalloys.

Alloys	Chemical composition (at%)									ρ (g/cm^3)
	Co	Ni	Al	W	Ta	Cr	Nb	B	C	
3Ta	Bal.	40	10	7.5	3	10	–	0.06	0.6	9.2
3Nb	Bal.	40	10	7.5	–	10	3.0	0.06	0.6	8.8

Structural characterization of the alloys was performed by X-ray diffraction (XRD) using Cu-Kα radiation. The 2θ range was set between 20° and 100°, using an angular incremental step of 0.02° and a counting time of 50 s/point. These measurements were performed at room temperature. During the solidification and cooling of the ingot a preferred orientation of grains was developed, due to a steep thermal gradient caused by the Cu crucible. To overcome the few quantity of grain population issue radiated by the X-ray, a spinner stage was used as a sample holder. Spinning of the sample increases the number of radiated grains improving the quality of the XDR measurement. The Inorganic Crystal Structure Database (ICSD) [24] was used for phase identification.

The microstructural features of the samples in the as-cast condition were analyzed by scanning electron microscopy (SEM) with a field emission gun model F50 Inspect from FEI. Semi-quantitative energy dispersion spectroscopy (EDS) was performed inside the grains and at the grain boundaries using an Oxford solid-state EDS detector. Electron backscattered diffraction (EBSD) was performed for phase identification of the minor phases (carbides and other intermetallic phases) formed in the as-cast alloys. The volume fraction of γ′ phase and of the minor phases present in both materials was determined using Image J software [25]. Twenty randomly taken images at 200,000 × (for the γ′ phase) and at 500 × (for the minor phases) were used for the calculations. Transmission electron microscopy (TEM) was performed to analyze the γ/γ′ structure using a FEI/Philips CM-200T TEM operating at 200 kV. Samples for TEM analysis were prepared by the focus ion beam (FIB) technique following standard procedures.

3. Results and discussion

3.1. Microstructural characterization of as-cast 3Ta and 3Nb alloys

3.1.1. 3Ta alloy

Fig. 1 presents the X-ray diffraction result of the as-cast 3Ta alloy in which reflections of γ, γ′ and M_6C phases were indexed. Fig. 2a depicts the microstructure of the as-cast 3Ta alloy that has a hardness of 442 ± 10 HV. Fig. 2b presents a TEM image in dark field condition showing the γ′ precipitates having a polyhedral morphology with a size ranging between 10 and 20 nm, with a measured volume fraction of 0.43. An electron diffraction pattern of the same region confirms that the indexed spots correspond to the γ/γ′ structure. Fig. 2c depicts the minor phases with a measured fraction of 0.06 with a fishbone-like morphology and enriched in Ta and W. A FIB lift-out sample of 3Ta alloy was taken out of a region containing a M_6C carbide precipitate. This sample was imaged using a TEM in bright field condition (Fig. 2d).

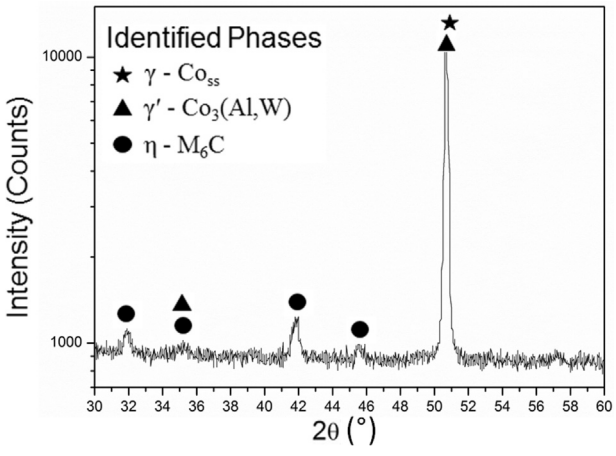

Fig. 1. X-ray diffractogram of the 3Ta as-cast alloy.

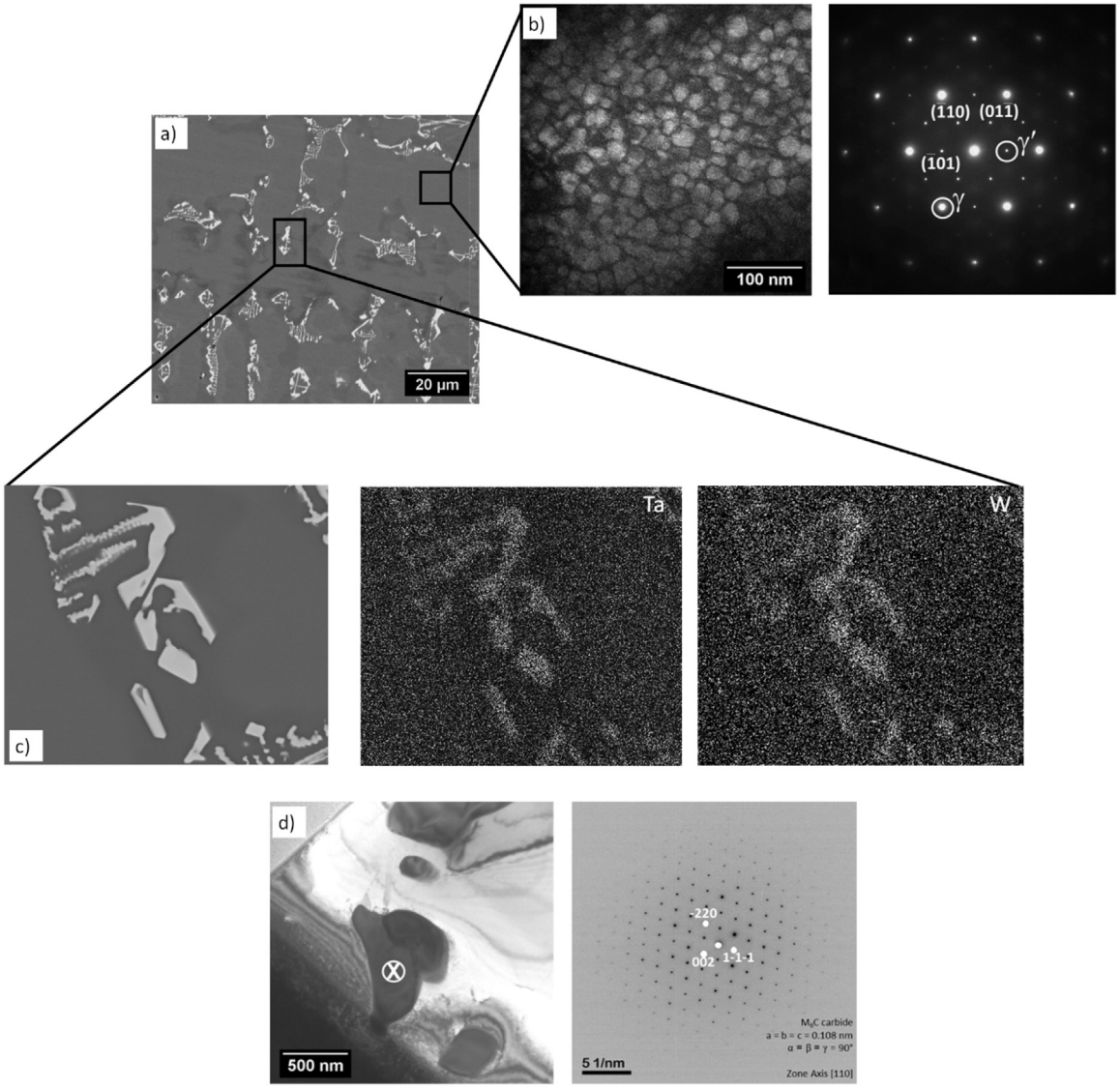

Fig. 2. a) A back scattered electron image showing the microstructure of 3Ta alloy in as-cast condition; b) TEM image in a dark field mode of the γ-γ′ structure and electron diffraction pattern from the same region in the [111] zone axis; c) fishbone-like precipitates and EDS mappings showing that these precipitates are rich in Ta and W; d) TEM image in a bright field condition and an electron diffraction pattern indexed as M_6C carbide.

The electron diffraction pattern obtained in the [110] zone axis confirms the presence of M_6C carbide. The formation of a primary eutectic γ/M_6C confirmed the prediction reported by Cacciamani et al.[21] showing only M_6C as a stable carbide in the Co-Ta-C system.

Fig. 3 shows the calculated solidification path determined using Scheil simulation. The simulation predicts the formation of γ and M_6C,

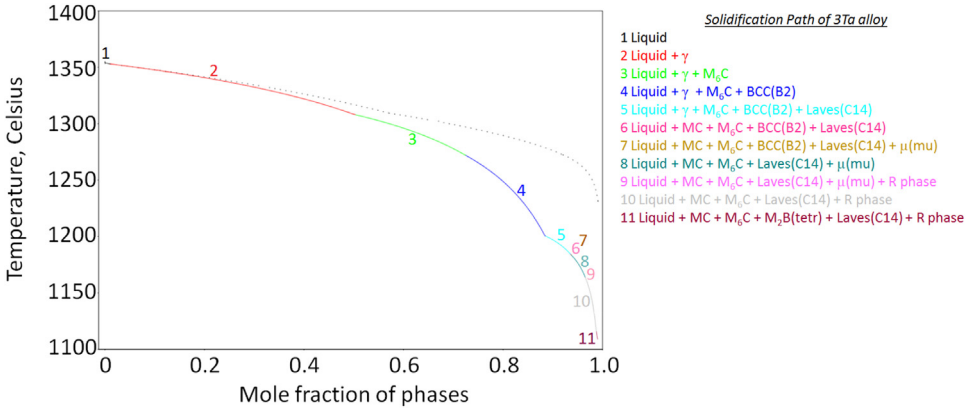

Fig. 3. The solidification path of 3Ta alloy simulated using Scheil model.

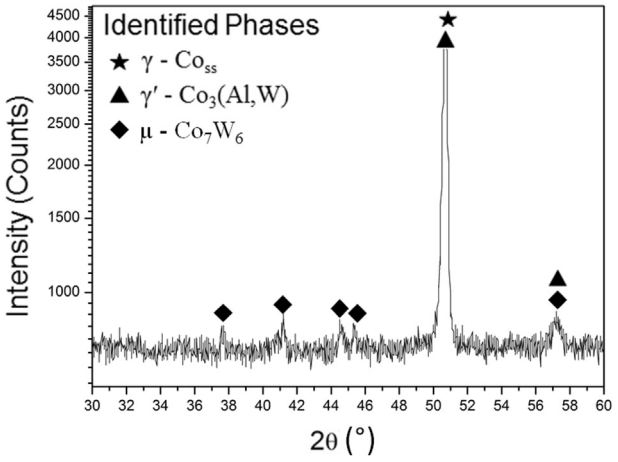

Fig. 4. X-ray diffractogram of the 3Nb as-cast alloy.

similar to what was observed in the previous results of microstructural analysis. Several other crystalline phases (such as Laves, MC and μ-Co_7W_6) were predicted to form. However, these were not found on the microstructural characterization of the as-cast 3Ta alloy. Scheil calculations are based on thermodynamic equilibrium observed only at solid/liquid interface, which suggested that the non-equilibrium solidification of the alloy occurred and the formation of the aforementioned phases could be suppressed.

3.1.2. 3Nb alloy

From the X-ray diffraction result for the 3Nb material, depicted in Fig. 4, the reflections of γ, γ′ and μ-Co_7W_6 phases were indexed. Fig. 5a depicts the as-cast microstructure of the 3Nb alloy that presents a hardness of 435 ± 12 HV. A dark field image obtained by TEM shows a γ/γ′ structure (Fig. 5b). An indexed selected area diffraction pattern of the same region confirmed the presence of both γ and γ′. The 3Nb alloy has a measured γ′ volume fraction of 0.43, with its size ranging from 10 to 20 nm. Fig. 5c depicts some minor phases that formed during the solidification process. EDS mapping show that W, Nb and Cr enrich these minor precipitates that have a measured volume fraction of 0.02. Phase identification results using EBSD analysis of minor phases formed in the 3Nb alloy are shown in Fig. 5d. The Kikuchi patterns of minor phases were indexed as MC carbide and μ-Co_7W_6 phase.

The calculated solidification path for the 3Nb alloy (Fig. 6) predicted the formation of γ, MC and μ-Co_7W_6, which showed a good agreement with experimental results. Minor precipitates such as M_6C, MC and μ-Co_7W_6 can be stabilized by Ta and Nb additions [26,27]. However, MC carbide and μ-phase were found only in 3Nb, whereas in 3Ta alloy only M_6C carbide precipitates were identified. The calculated solidification path by Scheil model predicted quite accurately the observed minor precipitates (MC and μ-Co_7W_6) in 3Nb alloy. For the 3Ta alloy, M_6C carbide was predicted and found experimentally. This confirmed that, according with the Scheil simulations, the 3Ta and 3Nb alloys followed different solidification paths.

3.2. Phase transformation temperatures

The multicomponent alloys studied in this work are quite complex systems when considering their microstructures. In order to identify the phase transformation temperatures at which reactions occurred in the as-cast 3Ta and 3Nb alloys, DSC measurements were performed. The experimental values were compared to the calculated transformation temperatures obtained by Scheil simulations that represent only the

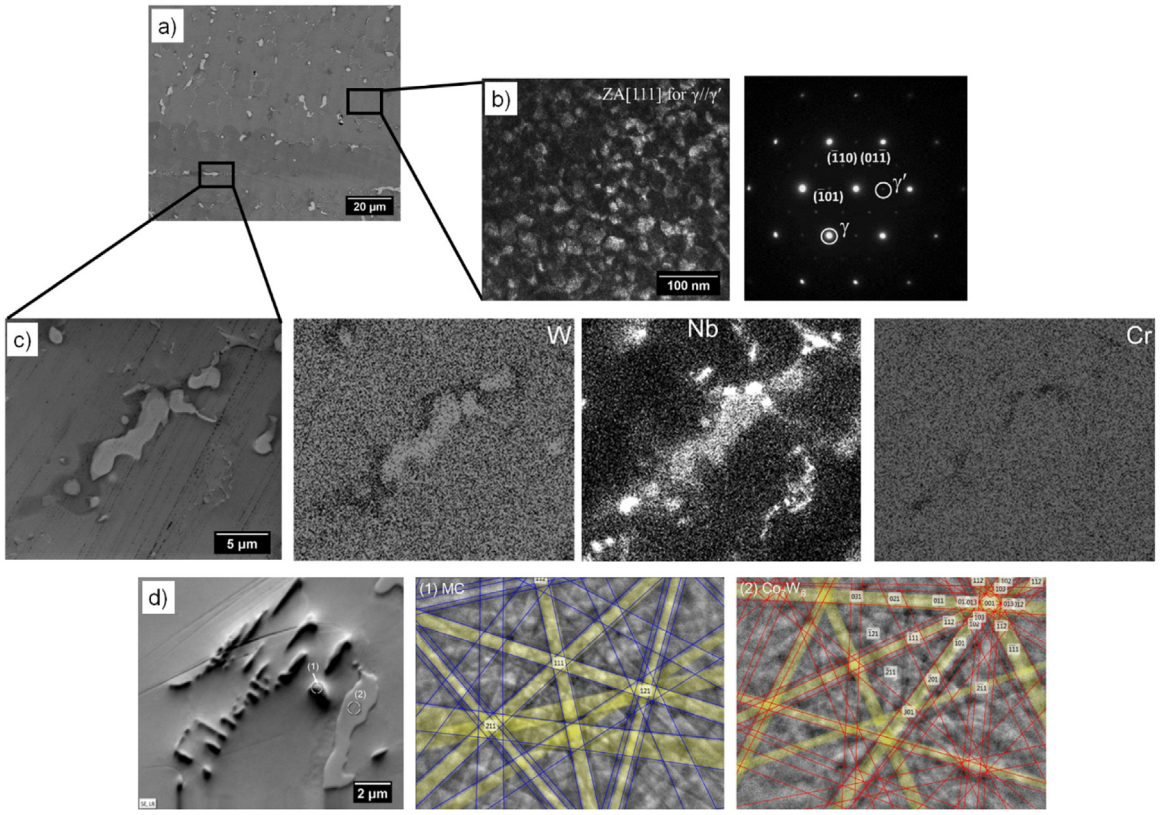

Fig. 5. a) A back scattered electron image showing the microstructure of 3Nb alloy in as-cast condition; b) TEM image in a dark field mode of the γ-γ′ structure and electron diffraction pattern from the same region in the [111] zone axis; c) SEM image of minor precipitates formed during the solidification process and EDS mappings of minor precipitates that are rich in W and Nb; and d) phase identification of minor precipitates using EBSD detector in which the indexed Kikuchi patterns of region 1 and 2 correspond to MC carbide and μ-Co_7W_6, respectively.

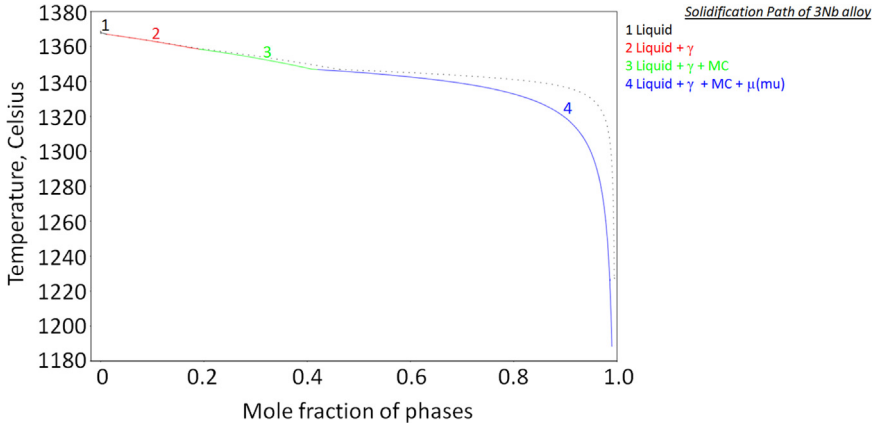

Fig. 6. The solidification path of 3Nb alloy simulated using Scheil model.

phase transformation path on which the liquid phase is involved. The γ′-*solvus* temperature was calculated in equilibrium conditions.

The solid-state reaction temperatures at which γ′ is dissolved into γ for the 3Nb and 3Ta alloys occurred at 1100 °C and 1143 °C, respectively. Our measurement of γ′-*solvus* temperature performed on both alloys were in good agreement with the reported results of Lopez-Galilea et al. [20] that determined the γ′-*solvus* temperature of an as-cast single crystal-SX Co-based superalloy by DSC. The calculated γ′-*solvus* temperatures for the 3Ta and 3Nb alloys were 1059 °C and 987 °C, respectively, as depicted in Fig. 7. As stated by Lass [22] the thermodynamic description of γ′ phase does not take into account the strong partition effect of Ta, Nb and Ti to γ′ which reflects on these important differences between the experimental and calculated γ′-*solvus*.

The M_6C carbide was predicted by Scheil simulation and found by microstructural characterization of the as-cast 3Ta alloy (Fig. 1c). The M_6C carbide was predicted to precipitate at 1309 °C. On the DSC heating curve, the onset temperature at which the 3Ta alloy started to melt was 1338 °C. This point could be related to the invariant temperature of the γ/M_6C eutectic transformation. This difference between calculated and experimental temperatures of M_6C carbide precipitation could be attributed to kinetic factors because these carbides are rich in heavy elements such as W and Ta, as shown by EDS mapping results (Fig. 1c). The calculated and experimental *liquidus* temperature were 1353 °C and 1378 °C, respectively.

On the microstructural characterization of the 3Nb alloy, MC carbide and μ-Co_7W_6 were identified. The experimental transformation temperatures of μ-Co_7W_6 and MC carbide were 1319 °C and 1359 °C, respectively. The calculated temperature formation of 1359 °C for the MC carbide showed a good agreement with the experimental value. For the μ-Co_7W_6 phase the calculated temperature was 1346 °C, which is slightly higher than the one measured. When in solid solution, Ni, Cr and Nb can affected the μ phase formation temperature. The calculated and experimental *liquidus* temperature were 1367 °C and 1378 °C, respectively. All phase transformation temperatures, experimental and calculated, are included in Table 2.

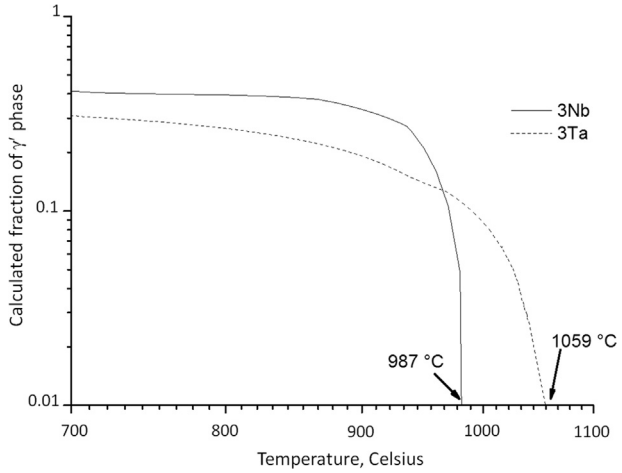

Fig. 7. The calculated γ′-*solvus* temperatures of 3Ta and 3Nb alloys in equilibrium condition.

3.3. Mechanical properties of 3Ta and 3Nb superalloys

Fig. 8 depicts the 0.2% yield stress obtained from hot compression tests for 3Ta, 3Nb, Mar M247 and B1914 alloys at different testing temperatures. Both 3Ta and 3Nb alloys have, at room temperature, a yield stress significantly higher than the one observed for the two Ni superalloys (Mar-M247 and B1914).

As claimed by Xu et. al [28], planar defects such as stacking faults were found in Ni-Co based superalloys deformed at low temperatures between 25–400 °C and its energy dramatically changed with Co content. The high content of Co added to 3Ta and 3Nb (28 at%) compared to 7.9 and 10 (at%) for Mar-M247 and B1914, respectively, lowers the stacking fault energy of the γCo_{ss}-matrix, reducing the dislocation mobility as well.

With increasing testing temperature an opposite relationship between yield stress and temperature was noticed. At 600 °C the value of yield stress for the 3Nb alloy was 787 MPa. Such value decreased to 756 MPa and 718 MPa to 750 °C and 850 °C, respectively. For the same temperature range the 3Ta alloy presented a 0.2% yield stresses of 852, 758 and 772 MPa.

From 25–600 °C, the 3Ta alloy showed a higher yield stress when compared to the 3Nb alloy. A minimum difference between yield stress values (3Ta with 758 MPa and 3Nb with 756 MPa) was observed at 750 °C. A peak of yield stress was not observed for the 3Nb alloy and a drop of this property (718 MPa and 708 MPa) between 850 and 950 °C

Table 2
The transformation temperatures of 3Ta and 3Nb alloys obtained experimentally by DSC and calculated by Scheil (S) and in equilibrium condition (e).

Temperature transformations (°C)	3Ta		3Nb	
	Calculated	DSC	Calculated	DSC
Liquidus	1353$^{(S)}$	1378	1367$^{(S)}$	1378
M_6C	1309$^{(S)}$	1338	–	–
MC	–	–	1359$^{(S)}$	1359
μ-Co_7W_6	–	–	1346$^{(S)}$	1319
γ′ *solvus*	1059$^{(e)}$	1143	987$^{(e)}$	1100

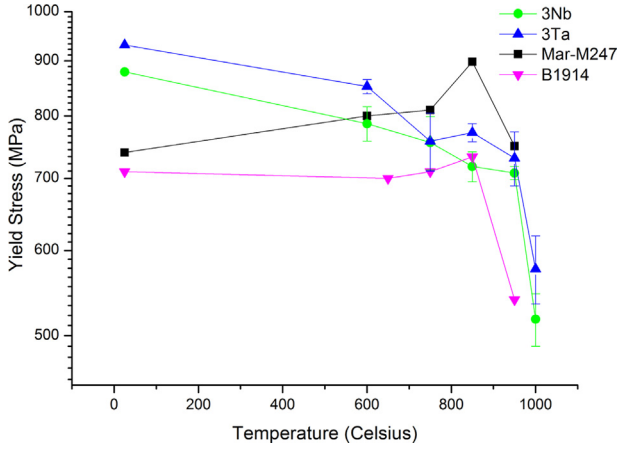

Fig. 8. The 0.2% yield stress (MPa) results for the Co-Ni based superalloys (3Nb and 3Ta alloys), and the two Ni based superalloys (Mar M247 and B1914).

was observed.

The 3Ta alloy presented a slight increase in the stress maxima (by 14 MPa) at 850 °C. This increase of the peak value was lower compared to the values obtained for Mar-M247 (88 MPa) and B1914 (23 MPa) alloy. Even though low increase of peak stress was observed in the 3Ta alloy, this material presented a higher yield stress compared to the Ta alloyed and W-free Co based alloy (30Ni-2Ta; 560 MPa) and a similar value to that of 30Ni-2Ti-2Ta (740 MPa), which were both hot tested at 870 °C in [14].

From 950–1000 °C a drop of yield stress took place in both alloys. This behavior could be correlated to the simulation results of the evolution of the γ′-fraction for 3Ta and 3Nb alloys, shown in Fig. 7. As the temperature exceeds 850 °C, the calculated fraction of γ′ phase for 3Nb and 3Ta alloys started to decrease more significantly. This trend is more prominent for 3Nb material, in which its γ′-fraction dropped sharply above 900 °C, whereas for 3Ta alloy a decrease of γ′-fraction took place steadily. In these conditions, Ta alloyed materials (3Ta and Mar-M247) showed higher values of yield stress compared to Nb-alloyed (3Nb alloy) and B-1914 alloys. The Ta addition to Co and Co-Ni based superalloys are considered to be effective in improving the thermal stability of γ′ [14–16] and due to its preferential partition to planar defects, such as superlattice intrinsic stacking fault [29], leading to an improvement in the mechanical strength during hot deformation [30–32].

At 1000 °C, 3Ta alloy showed a yield stress of 577 MPa which was higher than the yield stress of 3Nb alloy (518 MPa). The simulation results showed that at 1000 °C the γ′ phase was completely dissolved for the 3Nb alloy. However, it was shown experimentally by DSC (Table 2) that γ′ phase was stable for both alloys above 1000 °C. Even though the yield stress dropped at 1000 °C for 3Ta and 3Nb alloys, their values were kept above 500 MPa, with the presence of γ′ acting as the main strengthening phase guarantying the good performance behavior at high temperatures.

4. Conclusions

In this work the microstructural and mechanical characterization of two arc melted Co-Ni-Al-W based superalloys containing: i) Ta and ii) Nb was performed. The following main conclusions were drawn:

(1) Even though Ta and Nb can stabilize γ′, M_6C, MC and μ phases, a different solidification path was observed for both materials due to the fast cooling conditions during arc melting which favors the formation of non-equilibrium microstructures. These results were confirmed by Scheil simulations and microstructural characterization.

(2) A fair correlation was observed between the measured and calculated phase transformation temperatures for the minor phases found in both 3Ta and 3Nb alloys. However, some discrepancies between the calculated and experimental γ′-*solvus* temperatures for 3Ta and 3Nb alloys reflect that the thermodynamic description of γ′ phase does not consider accurately the strong partition effect of Ta, Nb and Ti into γ′.

(3) The 0.2% yield stress was obtained by hot compression tests for the 3Ta and 3Nb alloys and was compared to other polycrystalline Ni-based superalloys. The 3Ta alloy presented the highest yield stress values. The γ′ phase was stable for both alloys up to 1000 °C, being a good reason for 3Ta and 3Nb alloys presenting the yield strength above 500 MPa.

Acknowledgements

The authors acknowledge FAPESP (State of Sao Paulo Research Foundation) for financial support and fellowships (Process Number 2014/13772-4). The authors appreciate all experimental support provided by LNNano (CNPEM/MCTI) and a recognize special thanks to Dr. Johnnatan Rodriguez for his help in SEM/EBSD analysis.

References

[1] T.M. Pollock, Alloy design for aircraft engines, Nat. Mater. 15 (2016) 809–815, http://dx.doi.org/10.1038/nmat4709.
[2] K.C. Antony, Wear-Resistant Cobalt-Base Alloys, JOM 35 (1983) 52–60, http://dx.doi.org/10.1007/BF03338205.
[3] D. Coutsouradis, A. Davin, M. Lamberigts, Cobalt-based superalloys for applications in gas turbines, Mater. Sci. Eng. 88 (1987) 11–19, http://dx.doi.org/10.1016/0025-5416(87)90061-9.
[4] K. Shinagawa, H. Chinen, T. Omori, K. Oikawa, I. Ohnuma, K. Ishida, R. Kainuma, Phase equilibria and thermodynamic calculation of the Co–Ta binary system, Intermetallics 49 (2014) 87–97, http://dx.doi.org/10.1016/j.intermet.2014.01.015.
[5] G. Cacciamani, R. Ferro, I. Ansara, N. Dupin, Thermodynamic modelling of the Co-Ti system, Intermetallics 8 (2000).
[6] J.J. Ruan, C.P. Wang, C.C. Zhao, S.Y. Yang, T. Yang, X.J. Liu, Experimental investigation of phase equilibria and microstructure in the Co-Ti-V ternary system, Intermetallics 49 (2014) 121–131, http://dx.doi.org/10.1016/j.intermet.2014.01.011.
[7] H. Chinen, J. Sato, T. Omori, K. Oikawa, I. Ohnuma, R. Kainuma, K. Ishida, New ternary compound Co3(Ge, W) with L12 structure, Scr. Mater. 56 (2007) 141–143, http://dx.doi.org/10.1016/j.scriptamat.2006.09.007.
[8] J. Sato, Cobalt-Base High-Temperature Alloys, Science 312 (80) (2006) 90–91, http://dx.doi.org/10.1126/science.1121738.
[9] C.S. Lee, Precipitation-Hardening Characteristics of Ternary Cobalt - Aluminum - X Alloys, The University of Arizona, 1971, ⟨http://hdl.handle.net/10150/287709⟩.
[10] P. Wang, W. Xiong, U.R. Kattner, C.E. Campbell, E.A. Lass, O.Y. Kontsevoi, G.B. Olson, Thermodynamic re-assessment of the Al-Co-W system, Calphad Comput. Coupling Phase Diagr. Thermochem. 59 (2017) 112–130, http://dx.doi.org/10.1016/j.calphad.2017.09.007.
[11] J.J. Ruan, X.J. Liu, S.Y. Yang, W.W. Xu, T. Omori, T. Yang, B. Deng, H.X. Jiang, C.P. Wang, R. Kainuma, K. Ishida, Novel Co-Ti-V-base superalloys reinforced by L12-ordered γ′ phase, Intermetallics 92 (2018) 126–132, http://dx.doi.org/10.1016/j.intermet.2017.09.015.
[12] H.-.Y. Yan, V.A. Vorontsov, J. Coakley, N.G. Jones, H.J. Stone, D. Dye, Quaternary Alloying Effects and the Prospects for a New Generation of Co-base Superalloys, in: Superalloys, 2012: 2012: pp. 705–714. doi:10.1002/9781118516430.ch78.
[13] A. Suzuki, H. Inui, T.M. Pollock, L12-Strengthened Cobalt-Base Superalloys, Annu. Rev. Mater. Res. 45 (2015) 345–368, http://dx.doi.org/10.1146/annurev-matsci-070214-021043.
[14] S.K. Makineni, A. Samanta, T. Rojhirunsakool, T. Alam, B. Nithin, A.K. Singh, R. Banerjee, K. Chattopadhyay, A new class of high strength high temperature Cobalt based γ-γ′ Co-Mo-Al alloys stabilized with Ta addition, Acta Mater. 97 (2015) 29–40, http://dx.doi.org/10.1016/j.actamat.2015.06.034.
[15] T. Pollock, J. Dibbern, M. Tsunekane, J. Zhu, A. Suzuki, New Co-based γ-γ′ high-temperature alloys, JOM 62 (2010) 58–63.
[16] H.Y. Yan, V.A. Vorontsov, D. Dye, Alloying effects in polycrystalline γ′ strengthened Co-Al-W base alloys, Intermetallics 48 (2014) 44–53, http://dx.doi.org/10.1016/j.intermet.2013.10.022.
[17] J. Zhu, M.S. Titus, T.M. Pollock, Experimental investigation and thermodynamic modeling of the co-rich region in the Co-Al-Ni-W quaternary system, J. Phase Equilib. Diffus. 35 (2014) 595–611, http://dx.doi.org/10.1007/s11669-014-0327-5.
[18] J. Koßmann, C.H. Zenk, I. Lopez-Galilea, S. Neumeier, A. Kostka, S. Huth, W. Theisen, M. Göken, R. Drautz, T. Hammerschmidt, Microsegregation and precipitates of an as-cast Co-based superalloy—microstructural characterization and

phase stability modelling, J. Mater. Sci. 50 (2015) 6329–6338, http://dx.doi.org/10.1007/s10853-015-9177-8.
[19] I. Ohnuma, K. Ishida, Phase diagrams as tools for advanced materials design- applications to non-ferrous alloys, Tecnol. Em Metal. Mater. E Min. 13 (2016) 46–63, http://dx.doi.org/10.4322/2176-1523.1085.
[20] I. Lopez-Galilea, C. Zenk, S. Neumeier, S. Huth, W. Theisen, M. Göken, The thermal stability of intermetallic compounds in an as-cast SX co-base superalloy, Adv. Eng. Mater. 17 (2015) 741–747, http://dx.doi.org/10.1002/adem.201400249.
[21] G. Cacciamani, G. Roncallo, Y. Wang, E. Vacchieri, A. Costa, Thermodynamic modelling of a six component (C-Co-Cr-Ni-Ta-W) system for the simulation of Cobalt based alloys, J. Alloy. Compd. 730 (2018) 291–310, http://dx.doi.org/10.1016/j.jallcom.2017.09.327.
[22] E.A. Lass, Application of computational thermodynamics to the design of a Co-Ni-based γ′-strengthened superalloy, Metall. Mater. Trans. A. 48 (2017) 2443–2459, http://dx.doi.org/10.1007/s11661-017-4040-y.
[23] Thermo-Calc, TCNI8: TCS Ni-based Superalloys, (n.d.)8.
[24] F.I.Z. Karlsruhe, ICSD (Inorganic Crystal Structure Database) Scientific Manual, 1.1 (2008), p. 14.
[25] C.A. Schneider, W.S. Rasband, K.W. Eliceiri, NIH Image to ImageJ: 25 years of image analysis, Nat. Methods 9 (2012) 671–675, http://dx.doi.org/10.1038/nmeth.2089.
[26] O. Kruse, B. Jansson, K. Frisk, Experimental study of invariant equilibria in the Co-W-C and Co-W-C-Me (Me = Ti, Ta, Nb) Systems, J. Phase Equilib. 22 (2001) 552–555, http://dx.doi.org/10.1361/105497101770332703.
[27] L. Zhou, C.P. Wang, Y. Yu, X.J. Liu, H. Chinen, T. Omori, I. Ohnuma, R. Kainuma, K. Ishida, Experimental investigation and thermodynamic calculation of the phase equilibria in the Co–Nb–Ta ternary system, J. Alloy. Compd. 509 (2011) 1554–1562, http://dx.doi.org/10.1016/j.jallcom.2010.10.058.
[28] H. Xu, Z.J. Zhang, P. Zhan, C.Y. Cui, T. Jin, Z.F. Zhang, The synchronous improvement of strength and plasticity (SISP) in new Ni-Co based disc superalloys by controling stacking fault energy, Sci. Rep. (2017) 1–11, http://dx.doi.org/10.1038/s41598-017-07884-4.
[29] A. Mottura, A. Janotti, T.M. Pollock, Intermetallics A fi rst-principles study of the effect of Ta on the superlattice intrinsic stacking fault energy of L1 2 -Co 3 (Al, W), Intermetallics 28 (2012) 138–143, http://dx.doi.org/10.1016/j.intermet.2012.04.020.
[30] A. Bauer, S. Neumeier, F. Pyczak, R.F. Singer, M. Göken, Creep properties of different γ′-strengthened Co-base superalloys, Mater. Sci. Eng. A. 550 (2012) 333–341, http://dx.doi.org/10.1016/j.msea.2012.04.083.
[31] F. Xue, H.J. Zhou, Q. Feng, Improved high-temperature microstructural stability and creep property of novel Co-base single-crystal alloys containing Ta and Ti, JOM 66 (2014) 2486–2494, http://dx.doi.org/10.1007/s11837-014-1181-y.
[32] M.S. Titus, Y.M. Eggeler, T.M. Pollock, Creep-induced planar defects in L12 -containing Co- and CoNi-base single-crystal superalloys, ACTA Mater. 3 (2014) 1–10, http://dx.doi.org/10.1016/j.actamat.2014.08.033.